airfoil is very different from that of NACA 0012 airfoil. In case 3 we can see that the lower surface motion of NACA 4412 is identical with the upper surface motion as in case 1. Furthermore case 2 indicates that the turbulence intensity profiles of NACA 4412 airfoil are similar to those of NACA 0012 airfoil. Although leeward surfaces of two airfoils undergo downstroke motion, the turbulence intensity profiles have very small difference when lower surface shapes of airfoils are different. This reflects that very similar wake thickness and behavior of two airfoils is caused by the upward motion of the different lower surface shapes of NACA 0012 and NACA 4412. We thus conjecture that a small difference in the turbulence intensity profiles is noticed for different shapes of the airfoils as a result of the flow attachment to the leeward surface.

The significant difference of turbulence intensity profiles of two airfoils is shown in the wake region for the case of upstroke motion at $\alpha = -2$ deg (case 4). It is observed that the width of turbulence intensity is small for the NACA 0012 airfoil, whereas for NACA 4412 airfoil the width of turbulence intensity is much larger. When lower surface motion of NACA 4412 airfoil is identical with upper surface motion during the downstroke motion at $+\alpha$, the turbulence intensity in the wake region of lower surface is much larger than the other cases. This signifies that the flow is highly disturbed, so that the flow becomes very diffusive when the airfoil pitches up at a negative angle of attack. The difference in turbulence intensity of two airfoils is caused by both the different shape and the motion direction of lower surface.

Conclusions

Phase-averaged mean velocity and its fluctuations in the near wake of oscillating airfoils are presented. The near-wake characteristics of a NACA 0012 airfoil at $\pm\alpha$ show symmetric profiles about the X axis as a result of the symmetry of motion and airfoil shape. The velocity profiles and the turbulent intensity profiles of a NACA 4412 airfoil have small difference with those of a NACA 0012 airfoil except upstroke motion case at a negative angle of attack. These are attributable to either similar upper shape or the motion direction of the leeward surface, which result in the flow attachment to the surface. On the other hand, the significant difference of near-wake characteristics between NACA 0012 and NACA 4412 airfoil is observed in the case of upstroke motion at negative angle of attack. It is found that the streamwise velocity and turbulence intensity of the NACA 4412 airfoil in the wake region of lower surface are considerably large. These differences in streamwise velocity and turbulence intensity of two airfoils are caused by both the different lower shape and the motion direction.

References

[1]Hah, C., and Lakshminarayana, B., "Measurement and Prediction of Mean Velocity and Turbulence Structure in the Near Wake of an Airfoil," *Journal of Fluid Mechanics*, Vol. 115, 1982, pp. 251–282.

[2]Park, S. O., Kim, J. S., and Lee, B. I., "Hot-Wire Measurements of Near Wakes Behind an Oscillating Airfoil," *AIAA Journal*, Vol. 28, No. 1, 1990, pp. 22–28.

[3]Ho, C. M., and Chen, S. H., "Unsteady Wake of a Plunging Airfoil," *AIAA Journal*, Vol. 19, No. 11, 1981, pp. 1492–1494.

[4]Koochesfahani, M. M., "Vortical Patterns in the Wake of an Oscillating Airfoil," *AIAA Journal*, Vol. 27, No. 9, 1989, pp. 1200–1205.

[5]Liiva, J., "Unsteady Aerodynamic and Stall Effects on Helicopter Rotor Blade Airfoil Sections," *Journal of Aircraft*, Vol. 6, No. 1, 1969, pp. 46–51.

[6]Kanevce, G., and Oka, S., "Correcting Hot-wire Readings for Influence of Fluid Temperature Variations," *DISA Information*, No. 15, Oct. 1993, pp. 21–24.

[7]Chang, J. W., and Park, S. O., "A Visualization Study of Tip Vortex Roll-up of an Oscillating Wing," *Journal of Flow Visualization and Image Processing*, Vol. 6, No. 1, 1999, pp. 79–87.

[8]Chang, J. W., and Park, S. O., "Measurements in the Tip Vortex Roll-up Region of an Oscillating Wing," *AIAA Journal*, Vol. 38, No. 6, 2000, pp. 1092–1095.

Side Force on an Ogive Cylinder: Effects of Surface Roughness

S. C. Luo* and K. B. Lua†
National University of Singapore, Singapore 119260, Republic of Singapore
and
E. K. R. Goh‡
DSO National Laboratories, Singapore 118230, Republic of Singapore

Nomenclature

A	=	axial distance from model nose tip
Cy	=	side force coefficient, $Fy/(0.5\rho U_\infty^2 S)$
$Cy(A)$	=	local side force coefficient, local side force/$(0.5\rho U_\infty^2\ D \sin^2\alpha)$
D	=	cylinder diameter
d_{particle}	=	average diameter of aluminum oxide particles
Fy	=	side force
I	=	turbulence intensity
P	=	pressure on model surface
P_∞	=	freestream static pressure
Re_D	=	Reynolds number, $U_\infty D/\nu$
S	=	model base area, $\pi D^2/4$
U	=	time-average freestream velocity
α	=	angle of attack
δ_N	=	tip half-apex angle
θ	=	azimuth angle around circular cross section measured from the most leeward position
ν	=	kinematic viscosity of fluid
ρ	=	density of fluid
ϕ	=	roll angle

Introduction

THE experiments reported in the present Note and a related Note[1] are the extension of earlier work,[2] which experimentally studies the effects of freestream turbulence on the side force acting on an ogive cylinder at high incidence. In Ref. 2, the results indicate that freestream turbulence has different effects on flow past the ogive cylinder set at different roll angles. This is probably caused by different (nonuniform) microsurface imperfections on the body. Another factor that could play an important role is the state of the boundary layer. An earlier study[3] has shown that a boundary layer that is at/near a state of transition, that is, near the critical Reynolds number, is more responsive to freestream turbulence and undergoes an early transition to become a turbulent boundary layer. This has been known to cause a reduction in the aerodynamic loading on the body.

In Ref. 2, because of the speed (and, hence, Reynolds number) limitation of the wind tunnel used, the boundary layer of the ogive cylinder in the experiment was not near the transition state and the freestream turbulence did not cause the boundary layer to go through an early transition. To work around the described limitation and bring the boundary layer to the desired transition state, the authors

Received 24 February 2002; revision received 30 April 2002; accepted for publication 1 May 2002.

*Associate Professor, Department of Mechanical Engineering, 10 Kent Ridge Crescent.

†Research Fellow, Department of Mechanical Engineering, 10 Kent Ridge Crescent.

‡Senior Member of Technical Staff, Aeronautic Systems Programme, 20 Science Park Drive.

of this Note decided to coat the surface of the ogive cylinder with roughness of known dimensions. This was done because early studies had shown that boundary-layer transition could be made to take place at a lower Reynolds number by roughening the surface of a two-dimensional, that is, very slender, cylinder.[4–6] Although this finding is based on essentially two-dimensional flow, the present authors felt that the idea is worth trying in the present case of three-dimensional flow past an inclined ogive cylinder because it has not been studied before. In the present experiment, aluminum oxide particles with an average diameter d_{particle} of 0.326 mm (hence, $d_{\text{particle}}/D = 0.0093$) were chosen as the surface roughness coating. This is based on the results of Fage and Warsap,[6] who reported that the critical Reynolds number was brought down to near 3.5×10^4 by coating particles of this size on a two-dimensional cylinder. To preserve the characteristics of the tip geometry, the first 1 cm of the model was not coated.

Experimental Apparatus and Techniques

The experiments were carried out in an open-loop suction wind tunnel with a rectangular cross section measuring 0.6 m (height) × 1.0 m (width). All of the measurements were conducted at a freestream velocity of 15 m/s, thus giving a Reynolds number (Re_D) based on the diameter ($D = 35$ mm) of the cylindrical section of the model of 3.5×10^4. The turbulence intensity of the empty wind tunnel was found to be about 0.23%. In the present experiment, the angle of attack α of the model was fixed at 50 deg. The side force generated reached its maximum at this angle of attack, and the number of pressure tapping stations on the model is sufficient to capture at least the first local side force peak.

The model used was fabricated from a solid aluminum bar and has a nose length of $3.5D$ and a body length of $12.5D$, where D is the (constant) diameter the cylindrical section and is equal to 35 mm. The tip half-apex angle δ_N is 16.25 deg. Pressure tapings are located at $1.5D$, $2D$, $3D$, $4D$, $5D$, and $6D$ from the sharp end of the model. All pressure measurements were carried out using two sets of 48-channel scanivalves equipped with ±0.3 psi (2.064 kPa) pressure transducers with an accuracy of ±0.2% of the full scale. This translates into a maximum error of ±0.037 for the pressure coefficient at a freestream wind speed of 15 m/s. The side force was measured with a Nitta six-degree-of-freedom force balance. The accuracy of the balance is ±1.16 gm, which corresponds to a maximum error of ±0.0891 for the side force coefficient at the operating speed of 15 m/s. A computer equipped with an Pentium II microprocessor was used to both acquire the data and to control the stepper motor. The experimental apparatus and procedure used in the present investigation were the same as those described by Luo et al.[2]

Results and Discussion

In this section, the results of the ogive nose cylinder coated with aluminum particles (from now on referred to as the rough surface model), when subjected to a smooth flow (turbulence intensity ≈ 0.23%), are analyzed and compared to the results of the original (smooth surface) ogive nose cylinder.

Figure 1 shows the side force distributions of the smooth and rough surface models. It is obvious from Fig. 1 that, although the rough surface model generally experiences a smaller side force, the fluctuations in the side force are considerably larger. The pressure distributions of the smooth and rough models at a roll angle ϕ of 28.8 deg and at the pressure measuring station closest to the peak of local side force (station 3 in Fig. 2a) are shown in Fig. 2b. The results appear to indicate that the surface roughness has successfully triggered the boundary layer to change from a laminar to a turbulent state, as can be deduced from the associated pressure distributions. (It is known from bluff-body aerodynamics studies that a turbulent boundary layer on a cylinder has large negative pressure on its side, followed by steep pressure recovery.) Also note that although the surface roughness appeared to have succeeded in triggering the boundary layers on both sides of the model to the turbulent state, the flow asymmetry remains, and a nonzero side force, albeit somewhat smaller in magnitude, still exists.

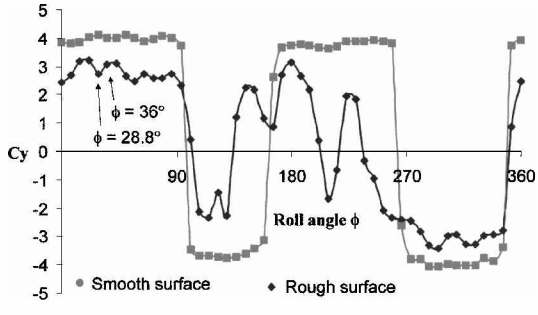

Fig. 1 Side force distributions of the smooth and rough surface models at $\alpha = 50$ deg.

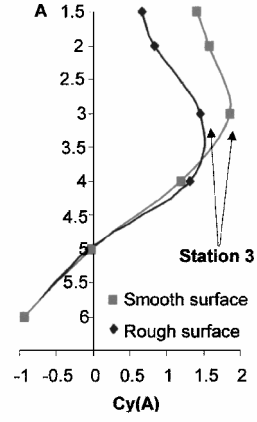

Fig. 2a Local side force distributions for the smooth and rough surface models at $\phi = 28.8$ deg.

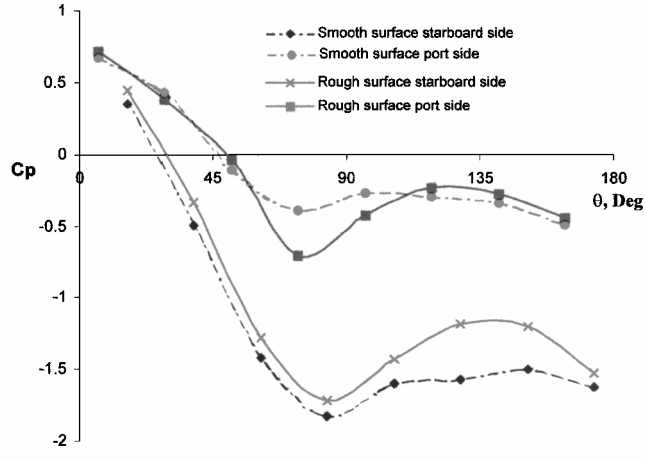

Fig. 2b Pressure distributions at station 3 of the smooth and rough surface model at $\phi = 28.8$ deg.

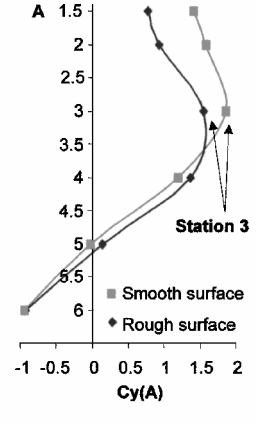

Fig. 3a Local side force distributions for the smooth and rough surface models at $\phi = 36$ deg.

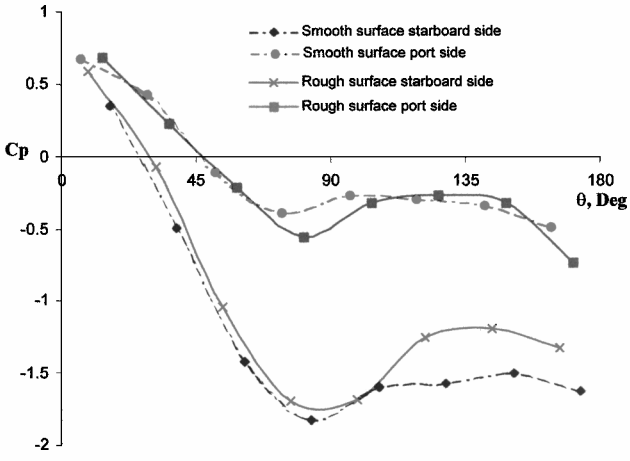

Fig. 3b Pressure distributions at station 3 for the smooth and rough surface model.

When flow past a normal circular cylinder near the critical Reynolds number was studied, Bearman[7] reported that there exists a small range of Reynolds number where a laminar separation bubble is formed on only one side of the cylinder, resulting in a large time-average lift (transverse) force. At a later time, Ericsson and Reding[8] reported that a very large side force occurs in the critical Reynolds number regime, where the body experiences subcritical (laminar) vortex separation on one side and a critical (turbulent) separation on the other side. A similar situation is also observed in the present investigation. Figure 3b shows the pressure distribution at $\phi = 36$ deg and at the pressure tapping station closest to the peak of local side force (station 3 in Fig. 3a). For the rough model, the pressure distributions indicate that the separation on the port side is more like a laminar type, whereas at the starboard side, boundary layer is already turbulent, as indicated by the large pressure recovery in the approximate range of $110 < \theta < 125$ deg. However, despite the difference in boundary-layer state between the two sides of the cylinder, note that the large side force is predominantly caused by the pressure difference between the two sides resulting from the flow asymmetry and only to a much smaller extent by the difference in state between the two boundary layers.

Conclusions

Effects of surface roughness on the side force acting on an ogive cylinder at high angle of attack have been studied. The present results show that the aluminium powder type of surface roughness used is capable of triggering the laminar to turbulent transition in the boundary layers of the ogive cylinder. This results in a side force that fluctuates more with roll angle, but is generally smaller (still nonzero) in magnitude. Closer examination of the circumferential pressure distribution reveals that, with the roughened surface, at certain roll angles, the boundary layer on both sides of the cylinder appear turbulent like; however, at other roll angles, only one of the two boundary layers is turbulent. However, for both cases, it was observed that the flow asymmetry at an angle of attack 50 deg remains and is the predominant cause of the large side force experienced by the ogive cylinder.

References

[1] Lua, K. B., Luo, S. C., and Goh, E. K. R., "Side Force on a Rough-Surface Ogive Cylinder: Effects of Freestream Turbulence," *Journal of Aircraft* (submitted for publication).

[2] Luo, S. C., Lua, K. B., and Lim, T. T., "Side Force on an Ogive Cylinder: Effects of Freestream Turbulence," *AIAA Journal,* Vol. 39, No. 12, 2001, pp. 2409–2411.

[3] Howard, R. M., Rabang, M. P., and Roane, D. P., Jr., "Aerodynamic Effects of a Turbulent Flowfield on a Vertically Launched Missile," *Journal of Spacecraft*, Vol. 26, No. 6, 1989, pp. 445–451.

[4] Szechenyi, E., "Supercritical Reynolds Number Simulation for Two-dimensional Flow over Circular Cylinder," *Journal of Fluid Mechanics*, Vol. 70, Pt. 3, 1975, pp. 529–542.

[5] Achenbach, E., and Heinecke, E., "On Vortex Shedding from Smooth and Rough Cylinder in the Range of Reynolds Numbers 6×10^3 to 5×10^6," *Journal of Fluid Mechanics*, Vol. 109, 1981, pp. 239–251.

[6] Fage, A., and Warsap, J. E., Report and Memorandum 1283, Aeronautical Research Council, 1930.

[7] Bearman, P. W., "On Vortex Shedding from a Circular Cylinder in the Critical Reynolds Number Regime," *Journal of Fluid Mechanics*, Vol. 37, 1969, pp. 577–585.

[8] Ericsson, L. E., and Reding, J. P., "Steady and Unsteady Vortex Induced Asymmetric Loads on Slender Vehicles," *Journal of Spacecraft and Rocket*, Vol. 18, No. 2, 1981, pp. 97–109.